Two-loop functional renormalization group approach to the one- and two-dimensional Hubbard model

A. A. Katanin
Institute of Metal Physics, 620041 Ekaterinburg, Russia, and Max-Planck Institute für Festkörperforschung, 70569 Stuttgart, Germany
(Received 16 June 2008; revised manuscript received 11 September 2008; published 11 June 2009)

We consider the application of the two-loop functional renormalization group (fRG) approach to study the low-dimensional Hubbard model. This approach accounts for both the universal and nonuniversal contributions to the RG flow. While the universal contributions were studied previously within the field-theoretical RG for the one-dimensional Hubbard model with linearized electronic dispersion and the two-dimensional Hubbard model with flat Fermi surface, the nonuniversal contributions to the flow of the vertices and susceptibilities appear to be important at large momenta scales. The two-loop fRG approach is also applied to the two-dimensional Hubbard model with a curved Fermi surface and the van Hove singularities near the Fermi level. The vertices and susceptibilities in the end of the flow of the two-loop approach are suppressed in comparison with both the one-loop approach with vertex projection and the modified one-loop approach with corrected vertex projection errors. The results of the two-loop approach are closer to the results of one-loop approach with the projected vertices, the difference of the results of one- and two-loop fRG approaches decreases when going away from the van Hove band filling. The quasiparticle weight remains finite in two dimensions at not too low temperatures above the paramagnetic ground state.

DOI: 10.1103/PhysRevB.79.235119 PACS number(s): 71.10.Fd, 71.10.Hf

I. INTRODUCTION

The discovery of high-T_c superconductors, which demonstrate nontrivial properties in a broad temperature and concentration range, has dramatically increased interest to correlated low-dimensional systems, and investigation of these systems have became a challenge for modern solid-state physics. Later discovery of unconventional triplet superconductors (in particular Sr_2RuO_4) has attracted further attention to possible instabilities of a Fermi-liquid state in the low-dimensional systems due to electronic correlations. These compounds stimulate theoretical interest to study the effect of correlations on electronic and magnetic properties of low-dimensional systems.

The common model which treats electronic correlations is the one-band Hubbard model. At sufficiently large on-site Coulomb repulsion $U \sim W$ (W is the bandwidth) this model describes the Mott metal-insulator transition. This transition is an essentially nonperturbative phenomenon and is well described by the dynamical mean-field theory,[1] which considers the limit of infinite number of dimensions and neglects spatial correlations. However, even in the weak- and intermediate-coupling regime $U < W$ properties of the Hubbard model are nontrivial in two dimensions near some special [van Hove (vH)] band fillings or Fermi surface nesting, where magnetic and/or superconducting instabilities may arise.[2] The spatial correlations, not considered in the dynamical mean-field theory, become important in the vicinity of the corresponding quantum phase transitions. Therefore, the development of methods, which are able to describe magnetic or superconducting fluctuations, is of high interest.

While the one-dimensional (1D) Hubbard model is exactly solvable by the Bethe ansatz and the phase diagram of this model with linearized electronic dispersion was obtained within the bosonization and field-theoretical renormalization group methods,[3] numerical or approximate analytical methods have to be used in higher dimensions. The applicability of numerical methods (exact diagonalization, quantum Monte Carlo, dynamical cluster approximations, etc.) which treat spatial correlations is restricted by the cluster size and/or not too low temperatures.

At the same time, there are a number of different (semi-) analytical approximations which treat the Hubbard model in the weak- and intermediate-coupling regime. The simplest is the mean-field approximation which treats the electron-electron interaction via some effective field applied to the fermionic system.[2] Regarding the stability of the paramagnetic state this approach is essentially equivalent to the requirement that in the absence of instabilities in the particle-hole (ph) or particle-particle (pp) channel, the corresponding susceptibilities in the random phase approximation (RPA) or T-matrix approximation (TMA) (Ref. 4) remain positive and finite. The corresponding electron-electron interaction vertex irreducible in the ph or the pp channel is supposed to be equal to the bare on-site Coulomb repulsion U in these approaches.

More complicated approaches account for the effect of fluctuations. These approaches can be subdivided into two classes: (i) approaches which consider the effect of the renormalization of the ph- or pp-irreducible electron-electron interaction vertex and (ii) approaches which consider in addition to (i) the renormalization of the one-particle Green's functions. One of the approximations of the first class is the combination of RPA and TMA, which was proposed to account for both the ph and the pp scattering.[5,6] In particular, one can use the RPA vertex (instead of the bare U) as the pp-irreducible vertex in TMA,[5] or—vice versa— the TMA vertex, which is irreducible in particle-hole channel, instead of the bare vertex in RPA.[6] The two-particle self-consistent (TPSC) approximation[7] uses the RPA-type vertex with the effective interaction U_{ef} instead of the bare one; the U_{ef} is determined by the requirement of the fulfillment of sum rules.

The commonly used approximation of the class (ii) is the fluctuation exchange (FLEX) approximation.[8] This approximation uses the RPA interaction vertices but accounts for the renormalization of the one-particle Green's functions as well. Although using RPA vertices in this approximation violates Pauli principle (see, e.g., Refs. 7 and 9), considering more complex structure of the vertices beyond RPA allows to treat self-energy and vertex corrections on the same foot. This is done, in particular, in the parquet approach[9–11] which considers the contribution of different channels of electron scattering and their mutual interplay in the interaction vertex.[12] However, the practical application of this approach for systems with the dimensionality $d>1$ meets serious computational difficulties and was performed only in few cases.[11,13]

The above-mentioned approximations give a possibility to treat spatial correlations of the Hubbard model in the weak- and intermediate-coupling regime. However, the accuracy of the results obtained within these approximations can be hardly controlled. The recently proposed functional renormalization group (fRG) approaches[14–20] use a different strategy. Integrating out modes with quasiparticle (qp) energy $|\varepsilon_{\mathbf{k}}|\geq\Lambda$, where Λ is the cutoff parameter, one obtains a (formally exact) hierarchy of RG equations for the n-particle interaction vertices. This hierarchy is usually truncated by neglecting higher-order vertices. To leading (one-loop) order these equations neglect the six-point vertex and describe the renormalization of the two-particle electron-electron interaction vertices only. Therefore the one-loop fRG approach belongs to approximations of class (i). Unlike the RPA and TMA, however, different electron scattering channels are treated on the same footing within the fRG. In one dimension this approach allows to reproduce the results obtained earlier within the field-theoretical RG approach.[21] The results for the instabilities, flow of electron-electron interaction vertices, and phase diagrams of the standard,[15,17,18,20–22] as well as the extended[23] two-dimensional (2D) Hubbard model were also obtained at one-loop order.

The self-energy effects, which are not included in the one-loop calculations, can be consistently taken into account at the two-loop order. In one dimension these effects are shown to be crucially important to describe Luttinger liquid behavior.[3] The calculation of the scattering rates,[18] quasiparticle residues,[24] and the electronic self-energy[25,26] in two dimensions using vertices obtained in the one-loop approximation showed, however, that contrary to the 1D case the self-energy effects in 2D are generally less important; they can however lead to the pseudogap structures of the spectral functions (see e.g., Refs 25 and 26).

To estimate corrections to the one-loop approximation, the full calculation of the two-loop contributions to the flow of vertices is necessary. Contrary to the calculations at one-loop order, the two-loop corrections account partly for the frequency dependence of the vertices and their momentum dependence beyond the projection to the Fermi surface. Therefore, the two-loop calculations serve also as a test of the importance of the frequency and momentum dependences of the vertices. Finally, they provide information about quasiparticle weight, damping, and interaction-induced Fermi surface shifts.

Although the two-loop corrections were considered previously for 2D systems in Ref. 27 within the field-theoretical renormalization group approach, the application of this approach is limited to nearly flat Fermi surfaces and the electronic dispersion linearized near the Fermi surface. The advantage of the functional renormalization group approach is that it can be applied to both flat and curved Fermi surfaces with or without van Hove singularities since this method does not require universality of the scaling functions. The applicability of this approach for calculation of the two-loop corrections to scaling functions of the bosonic ϕ^4 model was investigated in Ref. 28 where the need to account for the momentum and frequency dependences of the vertices was emphasized. The treatment of this dependence numerically is, however, a rather difficult task.

In the present paper we use a slightly different method, which allows us to avoid considering momentum and frequency dependences of the higher-order vertices, calculate the two-loop corrections, and investigate their influence on the flow of the coupling constants, susceptibilities, and self-energies of the Hubbard model. We use the momentum-cutoff version of the fRG for the one-particle irreducible (1PI) functions, which is applicable in the vicinity of antiferromagnetic (AF) or superconducting phase.

The plan of the paper is as follows. In Sec. II we introduce and compare the one- and two-loop fRG approaches. In Sec. III we apply the two-loop fRG approach to the 1D and 2D Hubbard models and investigate the flow of the interaction vertices and susceptibilities in this approach. In the conclusion (Sec. IV), we discuss results of the paper and outline future perspectives of the method. The derivation of the two-loop equations is presented in the Appendix.

II. THE MODEL AND THE TWO-LOOP FRG APPROACH

We consider the Hubbard model

$$H=-\sum_{ij\sigma}t_{ij}c^{\dagger}_{i\sigma}c_{j\sigma}+U\sum_{i}n_{i\uparrow}n_{i\downarrow}-\mu-4t\prime n, \tag{1}$$

where the hopping amplitude $t_{ij}=t$ for nearest neighbor sites i and j and $t_{ij}=-t'$ for next-nearest-neighbor sites $(t,t'>0)$; μ is the chemical potential, corresponding to the particle number n. In momentum space Eq. (1) reads

$$H=\sum_{\mathbf{k}\sigma}\varepsilon_{\mathbf{k}}c^{\dagger}_{\mathbf{k}\sigma}c_{\mathbf{k}\sigma}+\frac{U}{2N}\sum_{\mathbf{k}_1\mathbf{k}_2\mathbf{k}_3\mathbf{k}_4}\sum_{\sigma\neq\sigma'}c^{\dagger}_{\mathbf{k}_1\sigma}c^{\dagger}_{\mathbf{k}_2\sigma'}c_{\mathbf{k}_3\sigma'}c_{\mathbf{k}_4\sigma}\delta_{\mathbf{k}_1+\mathbf{k}_2-\mathbf{k}_3-\mathbf{k}_4}, \tag{2}$$

where the Kronecker δ symbol ensures momentum conservation, $\varepsilon_{\mathbf{k}}$ is the electronic dispersion, and N is the number of sites.

To calculate physical properties of model (1) we apply the fRG approach with a sharp momentum cutoff (see, e.g., Ref. 24), which considers an effective action obtained by integrating out modes with the quasiparticle energy $|\varepsilon_{\mathbf{k}}|\geq\Lambda$, with Λ being the cutoff parameter. This procedure is especially convenient when there is no ferromagnetic instability developing in the weak-coupling regime [in two dimensions this implies $t'\lesssim 0.3t$ (see Refs. 20 and 29)]. In the case of a ferromag-

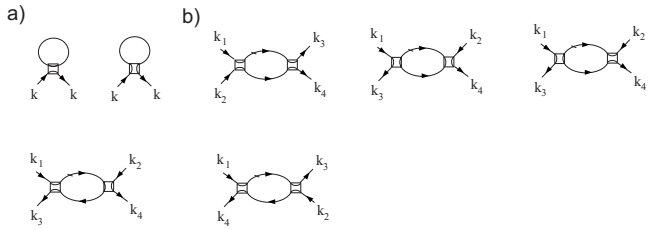

FIG. 1. The diagrams for the (a) self-energy and (b) vertex flow at the one-loop order. The solid lines correspond to the cut propagator G_Λ, the lines with dash to the single-scale propagator S_Λ, and the boxes to the vertices V_Λ. Lines inside the box show the direction of spin conservation.

netic instability the contribution of small-momenta particle-hole scattering which is not included in the momentum-cutoff fRG approaches may become important already at sufficiently large momenta scales;[20,29] this case is not considered in the present paper. Among different versions of the fRG approach [Polchinskii,[14,15] Wick-ordered,[16,17] or one-particle irreducible (1PI) (Refs. 18, 19, and 24)], we use the fRG approach for the 1PI functions, which is especially convenient for including the self-evergy effects. In this approach the electron propagator at scale Λ has the form

$$G_\Lambda(\mathbf{k},i\nu_n)=\frac{\theta(|\varepsilon_\mathbf{k}|-\Lambda)}{i\nu_n-\varepsilon_\mathbf{k}-\theta(|\varepsilon_\mathbf{k}|-\Lambda)\Sigma_\Lambda(\mathbf{k},i\nu_n)}, \tag{3}$$

where $\Sigma_\Lambda(\mathbf{k},i\nu_n)$ is the self-energy at the same scale; ν_n are the fermionic Matsubara frequencies. For $\Lambda\geq\Lambda_0=\max(|\varepsilon_\mathbf{k}|)$ the internal one-particle Green's functions in all the diagrams are zero so that the renormalization of the physical quantities is absent: the effective interaction V_Λ coincides with the bare one and $\Sigma_\Lambda(\mathbf{k},i\nu_n)=0$. The self-energy $\Sigma_\Lambda(\mathbf{k},i\omega_n)$ as well as the electron-electron interaction vertex $V_\Lambda(k_1,k_2;k_3,k_4)$ [$(k_1,\ k_2,\ k_3,$ and k_4 are the momenta and frequencies of the incoming and outgoing electrons, $k_i=(\mathbf{k}_i,i\nu_n^{(i)})$] at $\Lambda<\Lambda_0$ can be obtained by integration of the corresponding flow equations.

At one-loop order five diagrams contribute to the renormalization of the electron-electron interaction vertex $V_\Lambda(k_1,k_2;k_3,k_4)$ and two diagrams to the self-energy $\Sigma_\Lambda(\mathbf{k},i\nu_n)$ (see Fig. 1). The corresponding flow equations can be written in the form (see Refs. 18 and 19)

$$\frac{d\Sigma_\Lambda}{d\Lambda}=V_\Lambda\circ S_\Lambda, \tag{4a}$$

$$\frac{dV_\Lambda}{d\Lambda}=V_\Lambda\circ(G_\Lambda\circ S_\Lambda+S_\Lambda\circ G_\Lambda)\circ V_\Lambda, \tag{4b}$$

where $\circ$ is the short notation for the summation over momentum-, frequency- and spin variables according to standard diagrammatic rules (see diagrams of Fig. 1). The single-scale propagator $S_\Lambda(\mathbf{k},i\nu_n)$ is defined by

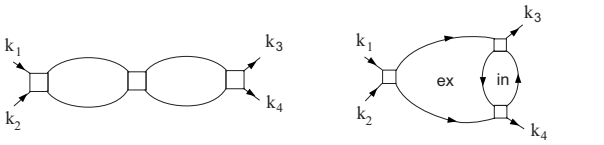

FIG. 2. Ladder-type (left) and nonladder (right) diagrams in the third-order perturbation theory. Solid lines correspond to the bare electronic propagator G_0, boxes to the bare interaction U, and in and ex denote internal and external bubble in the nonladder diagrams.

$$S_\Lambda(\mathbf{k},i\nu_n)=-\frac{\delta(|\varepsilon_\mathbf{k}|-\Lambda)}{i\nu_n-\varepsilon_\mathbf{k}-\theta(|\varepsilon_\mathbf{k}|-\Lambda)\Sigma_\Lambda(\mathbf{k},i\nu_n)}. \tag{5}$$

Equation (4) should be solved with the initial conditions $V_{\Lambda_0}=U$ and $\Sigma_{\Lambda_0}=0$. To demonstrate how the fRG [Eq. (4)] reproduce the perturbation theory results, it is helpful to expand their solution in the bare interaction U. To this end, we solve them iteratively. Starting from the bare values of V and Σ we obtain after one iteration the first-order result for the self-energy and the second-order perturbation theory (SOPT) result for the vertex

$$\Sigma_\Lambda^{(1)}=U\,\mathrm{Tr}(G_\Lambda^0),$$

$$V_\Lambda^{(1)}=U+U^2(G_\Lambda^0\circ G_\Lambda^0), \tag{6}$$

where the index "0" stands for the bare Green's functions with $\Sigma=0$. After the second iteration we have

$$\Sigma_\Lambda^{(2),1\text{-loop}}=U\,\mathrm{Tr}(G_\Lambda^{(1)})+U^2G_\Lambda^0\circ G_\Lambda^0\circ G_\Lambda^0,$$

$$V_\Lambda^{(2),1\text{-loop}}=U+U^2\int_\Lambda^{\Lambda_0}d\Lambda'[S_{\Lambda'}^{(1)}\circ G_{\Lambda'}^{(1)}+G_{\Lambda'}^{(1)}\circ S_{\Lambda'}^{(1)}]$$
$$+U^3[G_\Lambda^0\circ G_\Lambda^0\circ G_\Lambda^0\circ G_\Lambda^0]_\text{ladder}+U^3\int_\Lambda^{\Lambda_0}d\Lambda'$$
$$\times\left[(G_{\Lambda'}^0\circ G_{\Lambda'}^0)_\text{in}\circ\frac{d}{d\Lambda'}(G_{\Lambda'}^0\circ G_{\Lambda'}^0)_\text{ex}\right]_\text{non-ladder}. \tag{7}$$

Here the $G^{(1)}$ and $S^{(1)}$ functions are calculated with self-energy (6), "ladder" and "nonladder" denote two different kinds of diagrams (see Fig. 2), and "in" and "ex" denote the Green's functions which belong to the internal and external bubble in the nonladder diagrams, as shown in Fig. 2. The integrands in the second and last lines do not form a total Λ derivative, and therefore we do not obtain the exact third-order perturbation theory (TOPT) result for the vertex. While the integrand in the first line of the Eq. (7) can be changed to form the total derivative by the replacement $S_\Lambda\to dG_\Lambda/d\Lambda$, which was shown in Ref. 30 to be equivalent to borrowing some terms from the two-loop corrections to the vertex, casting the term in the third line of Eq. (7) to the form of the total derivative requires full consideration of the two-loop corrections.

The consideration above provides a definition of the n-loop approximation as an approximation which *correctly*

reproduces n-loop parts of the diagrams for the two-particle interaction vertex and $n+1$-loop parts of the self-energy diagrams. In the presence of logarithmic divergencies (e.g., in one dimension), when $G^0_\Lambda \circ G^0_\Lambda \sim \ln(\Lambda/\alpha)$ ($\alpha \ll \Lambda$ is a small parameter), the terms $(G^0_{\Lambda'} \circ G^0_{\Lambda'} \circ G^0_{\Lambda'}) \circ (dG^0_{\Lambda'}/d\Lambda')$ and $U^3(G^0_{\Lambda'} \circ G^0_{\Lambda'})_{\mathrm{ex}} \circ d(G^0_{\Lambda'} \circ G^0_{\Lambda'})_{\mathrm{in}}/d\Lambda'$ which appear at the two-loop order (see below) and are necessary to combine to the total derivatives in the Eq. (7) can be neglected to leading logarithmic order. This provides another more conventional definition of the n-loop approximation as an approximation which correctly treats the terms $U^m \ln^{m-n}(\Lambda/\alpha)$ in the perturbation series for the vertex ($m \geq n$). Note, however, that in two dimensions the bubbles $G^0_{\Lambda'} \circ G^0_{\Lambda'}$ are either nondivergent for arbitrary fillings or may contain squared logarithmical divergencies for some special (van Hove) band fillings, and the latter definition of the n-loop approximation cannot be applied.

To go beyond the one-loop order of Eq. (3) one has to take into account the contribution of the three-particle interaction vertex (see Refs. 18 and 19 and Appendix). Generally, this vertex generates contributions to the two-particle interaction vertex V with an arbitrary number of loops $n \geq 3$.[19] At this stage two different approximations are possible: (a) keep only contributions which are necessary to treat exactly diagrams with fixed number n of loops and (b) keep all the contributions which are generated by an integration of the equation for the $n+1$-particle vertex, neglecting $n+2$-particle vertex. In the present paper we restrict ourselves to approximation (a), i.e., consider only those contributions to RG flow which are necessary to treat exactly the two-loop parts of the diagrams.

At the two-loop order the flow equation for self-energy (4) does not change while 32 new diagrams contribute to the renormalization of the vertex (see Fig. 3). The resulting two-loop equations have the form (see Appendix for the derivation)

$$\frac{d\Sigma_\Lambda}{d\Lambda} = V_\Lambda \circ S_\Lambda, \tag{8a}$$

$$\frac{dV_\Lambda}{d\Lambda} = V_\Lambda \circ (G_\Lambda \circ S_\Lambda + S_\Lambda \circ G_\Lambda) \circ V_\Lambda + S_\Lambda \circ \int_\Lambda^{\Lambda_0} d\Lambda' V_{\Lambda'} \circ G_{\Lambda'} \circ V_{\Lambda'} \circ G_{\Lambda'} \circ V_{\Lambda'} \circ S_{\Lambda'}. \tag{8b}$$

The two-loop terms in the Eq. (8) arise from the contribution of six-point vertex. Following Refs. 24–26 and 31, two-loop contributions to the self-energy (sunriselike diagrams) can be obtained by reinserting the four-point vertex into Eq. (8a) (see below). Contrary to the one-loop approximation the frequency dependence of the vertex becomes essential at the two-loop order. This can be seen from the fact that to reproduce the TOPT result one needs to iterate Eq. (8b) twice. If one neglects the frequency dependence of the vertices, Eq. (8) fails to reproduce correct TOPT results. The necessity of taking into account the frequency and momentum dependence of the vertex was previously emphasized in the two-loop calculation of the β function of ϕ^4 theory[28] and the self-energy calculation in the 2D Hubbard model.[24–26,31]

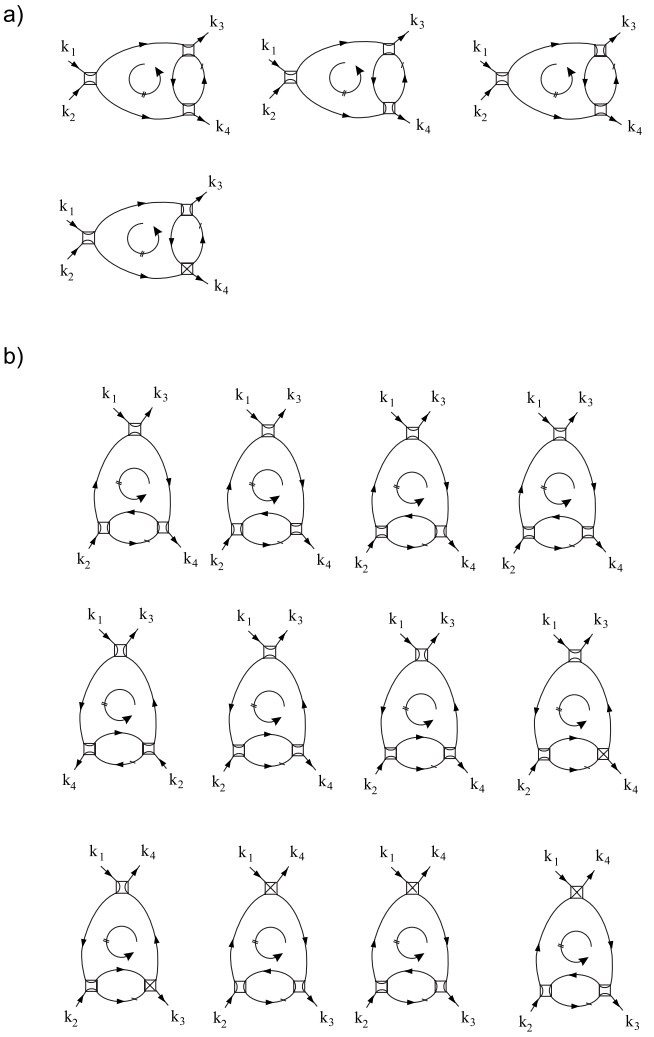

FIG. 3. The diagrams for the contributions to the flow of the vertex at the two-loop order in the (a) particle-particle and the (b) particle-hole channels. The two of the three lines without dash correspond to the $G_{\Lambda'}$ propagator and one to the $S_{\Lambda'}$ propagator (the circle arrow with double dash denotes their permutations). The line with dash corresponds to the single-scale propagator S_Λ. The other notations are the same as in Fig. 1.

To avoid having explicitly the frequency- and momenta-dependent vertices, we integrate Eq. (8b) formally and keep frequency and momentum dependences coming from the one-loop term only to obtain

$$V_\Lambda = \bar{V}_\Lambda + \delta V_\Lambda,$$

$$\delta V_\Lambda = \int_\Lambda^{\Lambda_0} d\Lambda' [V_{\Lambda'} \circ G_{\Lambda'} \circ S_{\Lambda'} \circ V_{\Lambda'} - \hat{\mathcal{P}}(V_{\Lambda'} \circ G_{\Lambda'} \circ S_{\Lambda'} \circ V_{\Lambda'})], \tag{9}$$

where $\bar{V}_\Lambda = \hat{\mathcal{P}} V_\Lambda$ and the operator $\hat{\mathcal{P}}$ projects the external fre-

quencies to zero and the external momenta to the Fermi surface. Reinserting this vertex into the one-loop contributions of Eq. (8) and using projected vertices in the two-loop contributions, we obtain to linear order in δV,

$$\frac{d\Sigma_\Lambda}{d\Lambda} = \bar{V}_\Lambda \circ S_\Lambda + S_\Lambda \circ \int_\Lambda^{\Lambda_0} d\Lambda' [\bar{V}_{\Lambda'} \circ G_{\Lambda'} \circ S_{\Lambda'} \circ \bar{V}_{\Lambda'} - \hat{\mathcal{P}}(\bar{V}_{\Lambda'} \circ G_{\Lambda'} \circ S_{\Lambda'} \circ \bar{V}_{\Lambda'})], \tag{10a}$$

$$\frac{d\bar{V}_\Lambda}{d\Lambda} = \hat{\mathcal{P}}\Big\{ \bar{V}_\Lambda \circ (G_\Lambda \circ S_\Lambda) \circ \bar{V}_\Lambda - \bar{V}_\Lambda \circ (G_\Lambda \circ S_\Lambda) \circ (\bar{V}_\Lambda^{1L} - V_0) + \bar{V}_\Lambda \circ (G_\Lambda \circ S_\Lambda) \circ \int_\Lambda^{\Lambda_0} d\Lambda' \bar{V}_{\Lambda'} \circ G_{\Lambda'} \circ S_{\Lambda'} \circ \bar{V}_{\Lambda'} + S_\Lambda \circ \int_\Lambda^{\Lambda_0} d\Lambda' \bar{V}_{\Lambda'} \circ G_{\Lambda'} \circ \bar{V}_{\Lambda'} \circ G_{\Lambda'} \circ \bar{V}_{\Lambda'} \circ S_{\Lambda'} \Big\}, \tag{10b}$$

where

$$\bar{V}_\Lambda^{1L} = V_0 + \hat{\mathcal{P}} \int_\Lambda^{\Lambda_0} d\Lambda' (\bar{V}_{\Lambda'} \circ G_{\Lambda'} \circ S_{\Lambda'} \circ \bar{V}_{\Lambda'})$$

is the analog of the one-loop vertex calculated with the two-loop vertices $\bar{V}_{\Lambda'}$. After this reinsertion, only the projected vertices $\bar{V}$ enter Eq. (10). While the last term in Eq. (10b) accounts for the two-loop corrections to the flow, other integral contributions correct the effect of the vertex projection in one-loop diagrams. In particular, for Λ-independent V and Σ the last two terms in Eq. (10b) combine to a Λ derivative of the corresponding two-loop diagram so that these equations with the initial condition $\bar{V}_{\Lambda_0}^{1L} = \bar{V}_{\Lambda_0} = V_0 \equiv U$, $\Sigma_{\Lambda_0} = 0$ correctly reproduce the result of the TOPT[32] after one iteration. The two-loop fRG equation for self-energy (10a) is identical to that investigated earlier with one-loop vertices.[25] The flow of the susceptibilities is described by the equation, similar to Eq. (10),

$$\frac{d\chi_\Lambda}{d\Lambda} = T_\Lambda \circ (G_\Lambda \circ S_\Lambda) \circ T_\Lambda, \tag{11a}$$

$$\frac{dT_\Lambda}{d\Lambda} = \hat{\mathcal{P}}\Big\{ T_\Lambda \circ (G_\Lambda \circ S_\Lambda) \circ \bar{V}_\Lambda - T_\Lambda \circ (G_\Lambda \circ S_\Lambda) \circ (\bar{V}_\Lambda^{1L} - V_0) + T_\Lambda \circ (G_\Lambda \circ S_\Lambda) \circ \int_\Lambda^{\Lambda_0} d\Lambda' \bar{V}_{\Lambda'} \circ G_{\Lambda'} \circ S_{\Lambda'} \circ \bar{V}_{\Lambda'} + S_\Lambda \circ \int_\Lambda^{\Lambda_0} d\Lambda' T_{\Lambda'} \circ G_{\Lambda'} \circ \bar{V}_{\Lambda'} \circ G_{\Lambda'} \circ \bar{V}_{\Lambda'} \circ S_{\Lambda'} \Big\}, \tag{11b}$$

with the initial condition $\chi_{\Lambda_0} = 0$ and T_{Λ_0} is determined by the symmetry of the order parameter, e.g., $T_{\Lambda_0} = 1$ for the antiferromagnetic and singlet superconducting (SSC) susceptibility, $T_{\Lambda_0}(k) = \cos k_y - \cos k_x$ for the d-wave superconducting (dSC) susceptibility etc.

Let us consider the local in Λ version of Eq. (10), which is obtained by the replacement $\bar{V}_{\Lambda'} \to \bar{V}_\Lambda$, $\Sigma_{\Lambda'} \to \Sigma_\Lambda$. This replacement introduces corrections of the same order, which are already neglected in the two-loop approximation and, therefore, can be considered on the same level of an approximation. In this way we obtain

$$\frac{d\Sigma_\Lambda}{d\Lambda} = \bar{V}_\Lambda \circ S_\Lambda + S_\Lambda \circ \bar{V}_\Lambda \circ [(1 - \hat{\mathcal{P}})(G_\Lambda \circ G_\Lambda)] \circ \bar{V}_\Lambda, \tag{12a}$$

$$\frac{d\bar{V}_\Lambda}{d\Lambda} = \hat{\mathcal{P}}\Big\{ \bar{V}_\Lambda \circ \frac{d}{d\Lambda}(G_\Lambda \circ G_\Lambda) \circ \bar{V}_\Lambda + \bar{V}_\Lambda \circ (G_\Lambda \circ S_\Lambda) \circ \bar{V}_\Lambda \circ [(1 - \hat{\mathcal{P}})(G_\Lambda \circ G_\Lambda)] \circ \bar{V}_\Lambda + S_\Lambda \circ \bar{V}_\Lambda \circ G_\Lambda \circ \bar{V}_\Lambda \circ G_\Lambda \circ \bar{V}_\Lambda \circ G_\Lambda \Big\}. \tag{12b}$$

Eq. (12) has a similar form as the two-loop equations in the field-theoretical approaches, e.g., for the 1D fermionic systems[3] and, therefore, can be used to make connection with these approaches. The terms with the projection operator $\hat{\mathcal{P}}$ coming from Eq. (9) subtract the one-loop ($\ln^2$ in 1D case) contributions from the third-order diagrams for the vertex. The corresponding contribution to the self-energy (last term in the first equation) is a frequency-independent constant, which can be omitted. Contrary to field-theoretical approaches, Eqs. (12a) and (12b) account for both, regular and singular terms in the perturbation expansion and are written for the coupling constants themselves, not for their invariant combinations with the self-energy.

To solve numerically Eq. (10) and (11), or (12), we use the discretization of momentum space in two patches (L and R) in one dimension and $N_p = 24$ patches in two dimensions with the same patching scheme as proposed in Ref. 20. For the frequency dependence of the self-energy we use $N_\omega = 100$ frequencies $i\nu_i$ suitably chosen on the imaginary axis [these frequencies do not have to coincide with the Matsubara frequencies since for a frequency-independent $\bar{V}$ the self-energy is defined on the entire imaginary axis (cf. Ref. 25)].

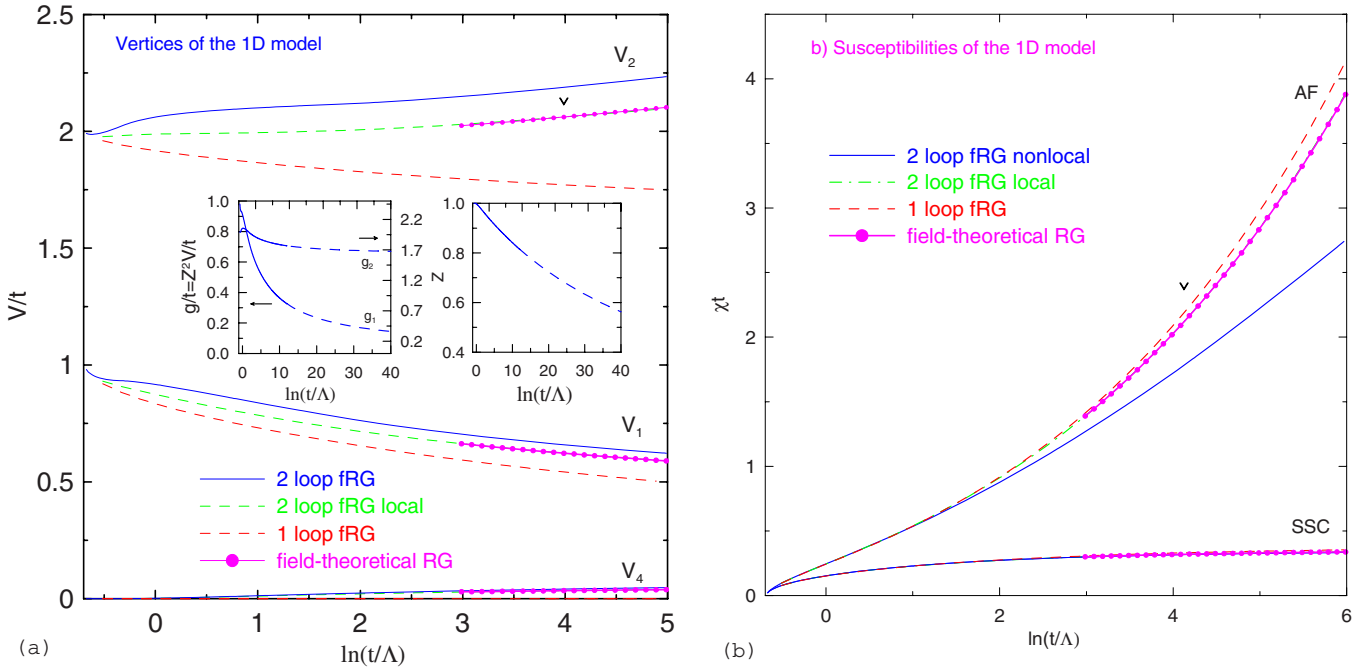

FIG. 4. (Color online) The flow of the (a) vertices, (b) the AF, and the SSC susceptibilities of the 1D Hubbard model within the nonlocal (solid lines) and local (dot-dashed lines) two-loop approaches and the one-loop approach (dashed lines). Insets show the flow of the invariant coupling constants $g_{1,2}=Z^2V_{1,2}$ and the quasiparticle residue Z, with dashed lines being the extrapolation of fRG results with $g_i=A+B/[C+\ln(t/\Lambda)]$. The results of the solution of field-theoretical two-loop Eq. (16) with initial vertices, obtained in the fRG approach at the scale $\Lambda=e^{-4}t$ (marked by arrow) are shown by bold lines with circles.

We account for the self-energy effects by expanding the self-energy $\Sigma_\Lambda(i\nu)$ around $\nu=0$ and introducing Z factors

$$Z^\Lambda_{\mathbf{k}_F}=[1-\partial\ \mathrm{Im}\ \Sigma_\Lambda(\mathbf{k}_F,i\nu)/\partial\nu]^{-1}_{\nu=0}. \tag{13}$$

The feedback of the imaginary part of the self-energy to the flow of vertices is neglected. The Green's functions in this approximation take the form[24]

$$G_\Lambda(\mathbf{k},i\nu_n)=\frac{Z^\Lambda_{\mathbf{k}_F}\theta(|\varepsilon_\mathbf{k}|-\Lambda)}{i\nu_n-\varepsilon_\mathbf{k}},$$

$$S_\Lambda(\mathbf{k},i\nu_n)=-\frac{Z^\Lambda_{\mathbf{k}_F}\delta(|\varepsilon_\mathbf{k}|-\Lambda)}{i\nu_n-\varepsilon_\mathbf{k}}, \tag{14}$$

where $\mathbf{k}_F$ corresponds to the projection of the vector $\mathbf{k}$ to the Fermi surface.

The derivative of the self-energy which enters Eq. (13) is determined numerically from the values of the self-energy at the first two frequencies $i\nu_{1,2}$. Approximation (14) can be applied only in the paramagnetic state without strong exchange and/or umklapp scattering (i.e., away from half filling in one dimension and at not too low temperatures and not too close to the van Hove band fillings in two dimensions). Above the antiferromagnetically ordered ground state the divergence of the corresponding vertices leads to a pseudogap structure of the self-energy and spectral functions.[25,26] This structure can be correctly described only with the frequency-dependent self-energy and is not considered here. The fulfillment of approximation (14) can be verified inspecting the frequency dependence of self-energy (10a) or (12a) at the imaginary axis during the flow and requiring that it is almost linear in frequency at small ν. The numerical checks show that this is indeed the case in the parameter range considered below. We also neglect the first and third terms in the flow equations for self-energies (10) and (12) as responsible purely for the deformation of the Fermi surface by the interaction. This deformation was found numerically to be small in two dimensions at small next-nearest hopping t' (Ref. 18) and can be treated accurately by introducing corresponding counterterms.[16,33,34]

III. RESULTS

A. 1D case

First we consider the results for the 1D electronic dispersion,

$$\varepsilon_k=-2t\cos k-\mu. \tag{15}$$

In this case we have only two patches (L and R) at $k_F=\pm\arccos(\mu/2)$. After the projection to the Fermi points, only four independent vertices remain: $V_1=V(L,R;R,L)$, $V_2=V(L,R;L,R)$, $V_3=V(L,L;R,R)$, and $V_4=V(L,L;L,L)=V(R,R;R,R)$. With the linearization of dispersion (15) near the Fermi points, the flow of these vertices in the two-loop approximation is well studied in the field-theoretical approach[3] and it is described by the following equations:

$$dg_1/dl=\frac{1}{\pi v_F}g_1^2+\frac{1}{2\pi^2v_F^2}g_1^2(g_1+g_4),$$

$$dg_2'/dl = \frac{1}{\pi v_F} g_3^2 + \frac{1}{2\pi^2 v_F^2} g_3^2 (g_1 - 2g_2 - g_4),$$

$$dg_3/dl = \frac{1}{\pi v_F} g_2' g_3 + \frac{1}{4\pi^2 v_F^2} g_3 [(g_2')^2 + g_3^2 - 2g_2' g_4],$$

$$dg_4/dl = \frac{3}{4\pi^2 v_F^2} (g_2' g_3^2 - g_1^3), \tag{16}$$

$$d \ln Z/dl = \frac{1}{4\pi^2 v_F^2} (g_1^2 - g_1 g_2 + g_2^2 + g_3^2), \tag{17}$$

where $g_i = Z^2 V_i$ are the invariant coupling constants, $g_2' = g_1 - 2g_2$, $v_F = 2t \sin k_F$, and $l = \ln \Lambda$. We emphasize once more that the difference of Eqs. (12) and (16) is that the latter accounts for the universal contributions to the flow of the coupling constants only, while the former treats also the nonuniversal contributions, e.g., connected with the nonlinearity of the dispersion.

The result of the solution of Eq. (12) for $g_1 = t$, $g_2 = 2t$, $g_3 = g_4 = \mu = 0$, and $T = 10^{-4} t$ is presented in Fig. 4. Similar to the field-theoretical approach[3] and previous one-loop fRG study,[31] the quasiparticle residue Z and the vertex g_1 asymptotically vanish in the limit $l \to \infty$, while the vertex g_2 approaches a constant value. To verify that the result of the solution of Eq. (16) is indeed reproduced at $\Lambda \ll 1$, we use the result of integration of Eq. (11) at some cutoff parameter $\Lambda_c = e^{-4} t \ll 1$ as a starting condition for Eq. (16) and compare the result of the solution of Eqs. (12) and (16) for $\Lambda < \Lambda_c$. One can see that the results of the local two-loop fRG approach agree with the corresponding results of the field-theoretical approach [Eq. (16)]. At the same time, the results of the solution of local and nonlocal fRG equations are different due to the nonuniversal initial part of the flow. We have verified that this is mainly connected with the momentum dependence of the Fermi velocity; the difference almost disappears for the linearized version of dispersion (15). Nonlocal Eq. (10a) is expected to treat better the effect of the nonlinearity of the dispersion; therefore, we consider only its solution in the 2D case below.

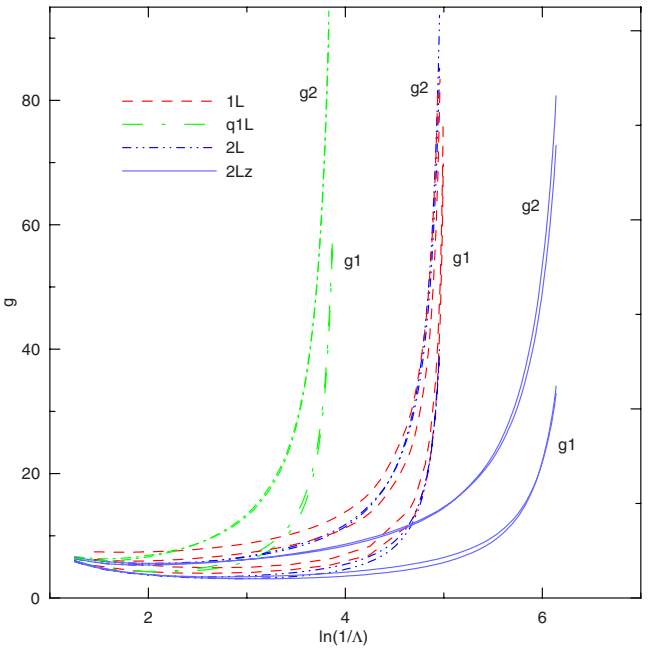

FIG. 5. (Color online) The flow of the vertices $g_1 = V(1,12,12)$ and $g_2 = V(1,12,12)$ of the 2D Hubbard model with the flat Fermi surface in the 24-patch one-loop approach with vertex projection (1*L*, dashed lines), the one-loop approach with partly corrected errors of the vertex projection (q1L, dot-dashed lines) and the two-loop approach with account of Z factors (2Lz, solid lines) and without Z factors (2L, dash-dot-dot lines). The 1st and 12th patches being closest to the centers of the opposite Fermi surface sides.

B. 2D case

For the discussion of the results of fRG approach in 2D case we also consider the solution of Eq. (10) without the two-loop corrections (i.e., without the last term in the second equation) to investigate how the one-loop flow changes due to correction of the errors of vertex projections by the second and third term in Eq. (10b). The difference of the latter results from the one-loop results shows the effect of the vertex projection on the renormalization group flows, while their difference to the two-loop results shows the effect of the two-loop corrections.

First we consider the results of the solution of Eq. (10) for the dispersion

$$\varepsilon_{\mathbf{k}} = -t(\cos p_x + \cos p_y) + t|\cos p_x - \cos p_y| - \mu. \tag{18}$$

The corresponding Fermi surface has flat parts along the directions $|p_x|, |p_y| = \arccos(-\mu/2)$. The field-theoretical approach for a flat Fermi surface was applied earlier in Refs. 27 and 35. The results of the numerical solution of Eq. (10) for $\mu = t$ and $U = 7.81t$ are shown in Fig. 5. We choose this relatively large value of the interaction U since it corresponds to the value of the dimensionless coupling constant $U\Delta/(\pi v_F) = 3$ used in Refs. 27 and 35, where v_F is the Fermi velocity and Δ is the length of the Fermi surface flat parts [$v_F = \sqrt{4t^2 - \mu^2}$ and $\Delta = 2 \arccos[-\mu/(2t)]$ for the dispersion (18)]; a larger value $U\Delta/(\pi v_F) = 10$ was considered in Ref. 27. One can see that the vertices without the two-loop corrections diverge at much larger energy scales compared to the two-loop results in agreement with Refs. 27 and 35. The scale of the vertex divergence in the one-loop approximation with partly corrected projection errors [Eq. (10) without the last term in the second equation] agrees with the result of the one-loop field-theoretical approach (not having any projection errors) but is larger than the corresponding scale in one-loop approach with vertex projection. The account of the vertex corrections (without the self-energy effects) shifts the scale of the divergence of the vertices almost to the scale of the one-loop approach with vertex projection. Further account of the self-energy corrections shifts the scale of the divergence of the vertices to a smaller scale than in the one-loop approximation with vertex projection. At large Λ far from the scale of the vertex divergence we obtain the behavior of the Z factors which is similar to the 1D case (not

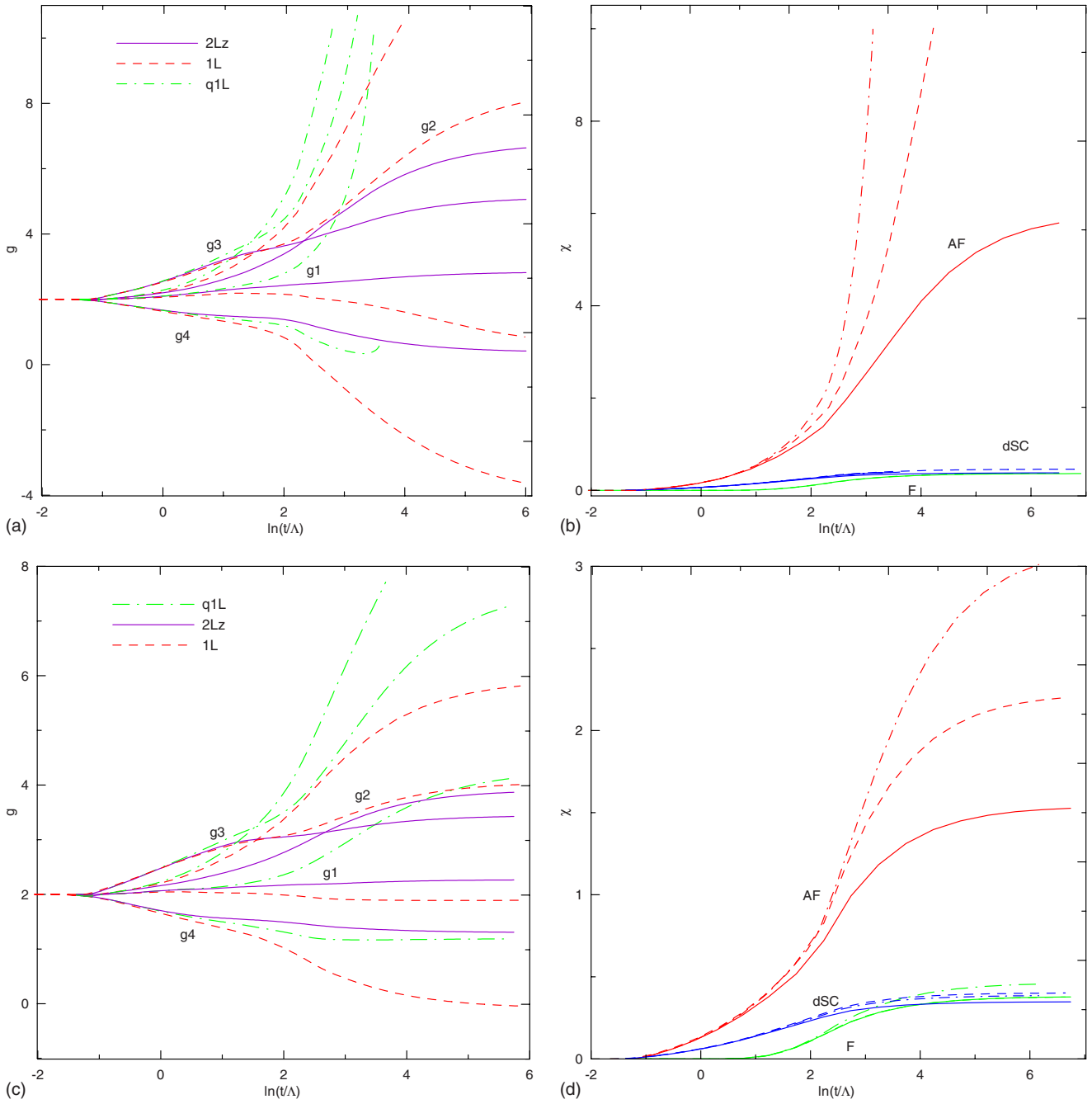

FIG. 6. (Color online) The flow of the (a) and (c) vertices $g_1=V(1,7,7)$, $g_2=V(1,7,1)$, $g_3=V(1,1,7)$, and $g_4=V(1,1,1)$, and (b) and (d) the AF, dSC, the ferromagnetic (F) susceptibilities of the 2D t-t' Hubbard model with $U=2t$, $t'/t=0.1$, $T=0.1t$, (a) and (b) $\mu=0.1t$, and (c) and (d) $\mu=-0.1t$ in the 24-patch one- and two-loop fRG approaches. The first and seventh Fermi surface patches correspond to points, closest to two different van Hove singularities. The solid lines in (b) and (d) correspond to the two-loop approach; the dashed lines to the one-loop approach with projected vertices, the dot-dashed lines to the one-loop approach with partly corrected errors of the vertex projections. Other notations are the same as in Fig. 5.

shown). Very close to the scale of the vertex divergence the Z factors are stronger suppressed, until the approximation of Eq. (14) breaks down. The flow of the vertices and quasiparticle weight in the two-loop approach agrees with the results of Refs. 27 and 35.

The functional renormalization group approach can be further applied to the $t-t'$ Hubbard model with the dispersion

$$\varepsilon_{\mathbf{k}} = -2t(\cos p_x + \cos p_y) + 4t'(\cos p_x \cos p_y + 1) - \mu, \tag{19}$$

where the conventional field-theoretical approach is not applicable due to the presence of squared logarithmic singularities in the perturbation series near van Hove band filling ($\mu=0$). The results for the flow of vertices and susceptibilities for $t'=0.1t$, $U=2t$, and the fillings close to vH band

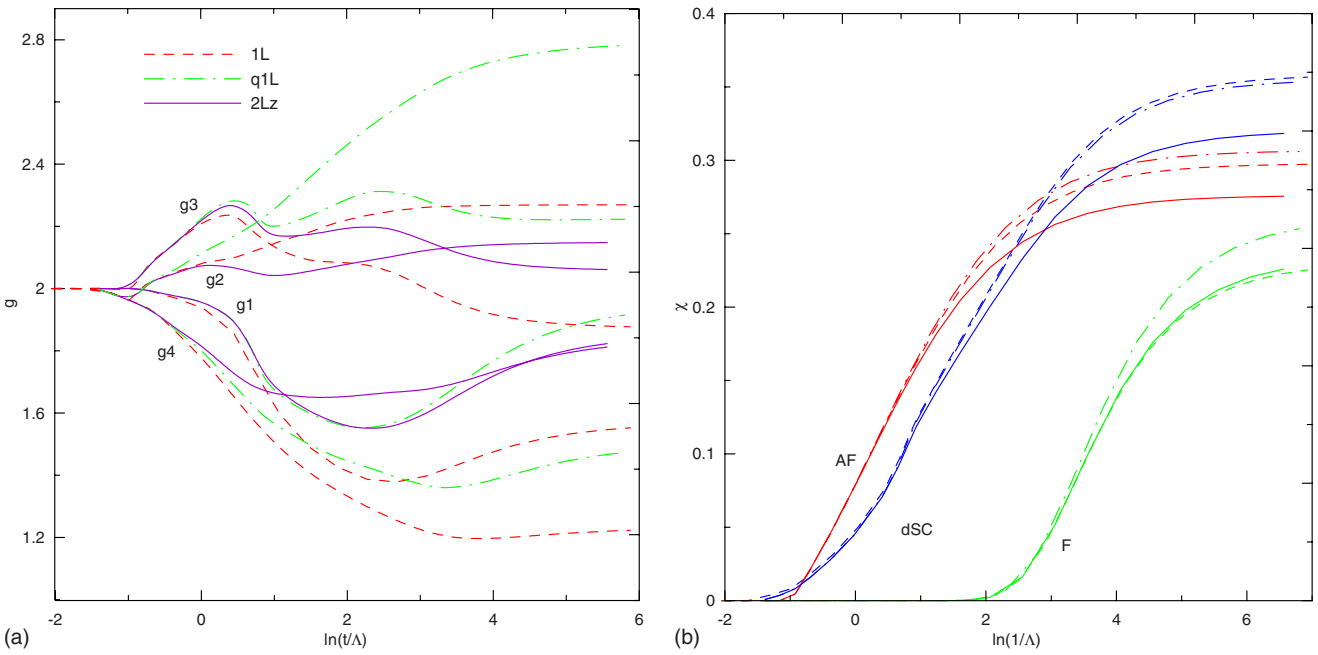

FIG. 7. (Color online) The flow of the (a) the vertices and the (b) the susceptibilities of the 2D t-t' Hubbard model, $U=2t$, $t'/t=0.1$, $\mu=-0.5t$, and $T=0.025t$ in the 24-patch one- and two-loop fRG approaches. The notations are the same as in Fig. 6.

filling ($\mu=\pm 0.1t$) are presented in Fig. 6. At $\mu=0.1t$ (above vH filling) the largest susceptibility is observed with respect to the antiferromagnetic instability in both the one- and the two-loop approaches. For this value of μ and chosen temperature $T=0.1t$ the results for the susceptibilities in one- and two-loop approach substantially differ. The antiferromagnetic susceptibility in the end of the flow in the one-loop approach with partly corrected errors of vertex projection [Eq. (10) with omitted last term in the second equation] is larger than the results of this approach with vertex projection and deviates more from the two-loop results. Therefore, the results of one-loop approach with vertex projection agree better with the two-loop results, which is possibly due to account of only universal terms of the flow in these approaches. For $\mu=-0.1t$ (below vH filling) we observe the same qualitative tendencies with smaller difference of the results of one- and two-loop approaches. With decreasing temperature, the superconducting instability becomes dominating in this case (see below).

The results for the flow of the vertices and susceptibilities at the filling further from vH one ($\mu=-0.5t$) are shown in Fig. 7. At this filling and not too low temperatures the antiferromagnetic susceptibility is the largest one (not shown), but with decreasing temperature the d-wave superconducting instability becomes the leading instability. Susceptibilities in the one-loop approach with partial correction of vertex projection errors are larger than the one- and the two-loop approaches. The susceptibilities in the end of the flow of one- and two-loop approaches are, however, closer to each other than in the above considered case $\mu=-0.1t$.

The calculated temperature dependences of the susceptibilities for antiferromagnetic and superconducting instabilities, as well as Z factors for $\mu=\pm 0.1t$, are shown in Fig. 8. At $\mu=0.1t$ we observe a maximum of the antiferromagnetic susceptibility in the two-loop approach, while the corresponding susceptibility in the one-loop approach diverges with decreasing temperature [Fig. 8(a)]. More generally, we find that the divergence of the vertices (and susceptibilities) is strongly suppressed in the two-loop approach. This divergence is not, however, fully removed since for smaller $\mu<0.08$ we find again the possibility of the antiferromagnetic ground state in the two-loop approach. At $\mu=-0.1t$ the antiferromagnetic susceptibility also has a maximum at some temperature and then decreases with decreasing T [Fig. 8(b)], while the superconducting susceptibility increases, showing the possibility of the superconducting ground state in both one- and two-loop approaches. The increase of χ_{dSC} in the one-loop approach is again more pronounced than in the two-loop approach so that the temperature where the susceptibility diverges in the two-loop approach is expected to be much smaller than in the one-loop approach. The Z factors decrease almost linearly with $\ln(t/T)$ at intermediate temperatures, but below the temperature, where the maximum of the susceptibility is reached, their temperature dependence becomes linear in T and therefore $Z_{\mathbf{k}_F}$ are not expected therefore to vanish at lower temperatures. We have also verified during the calculations that the imaginary part of the self-energy remains as linear function of ν at small imaginary frequencies.[36]

In Fig. 9 we summarize the results for the qp damping $\Gamma_{\mathbf{k}_F}=-\mathrm{Im}\,\Sigma(\mathbf{k}_F,0)$ and the Fermi surface shift $\mathrm{Re}\,\Sigma(\mathbf{k}_F,0)$ estimated at different Fermi surface points in the end of the two-loop fRG flow. The qp damping depends almost linearly on temperature at not too low temperatures; this dependence becomes quadratic at low T. The observed linear dependence of the scattering rates at not too low temperatures may be due to closeness to the antiferromagnetic quantum critical point; more detailed investigations of this dependence are,

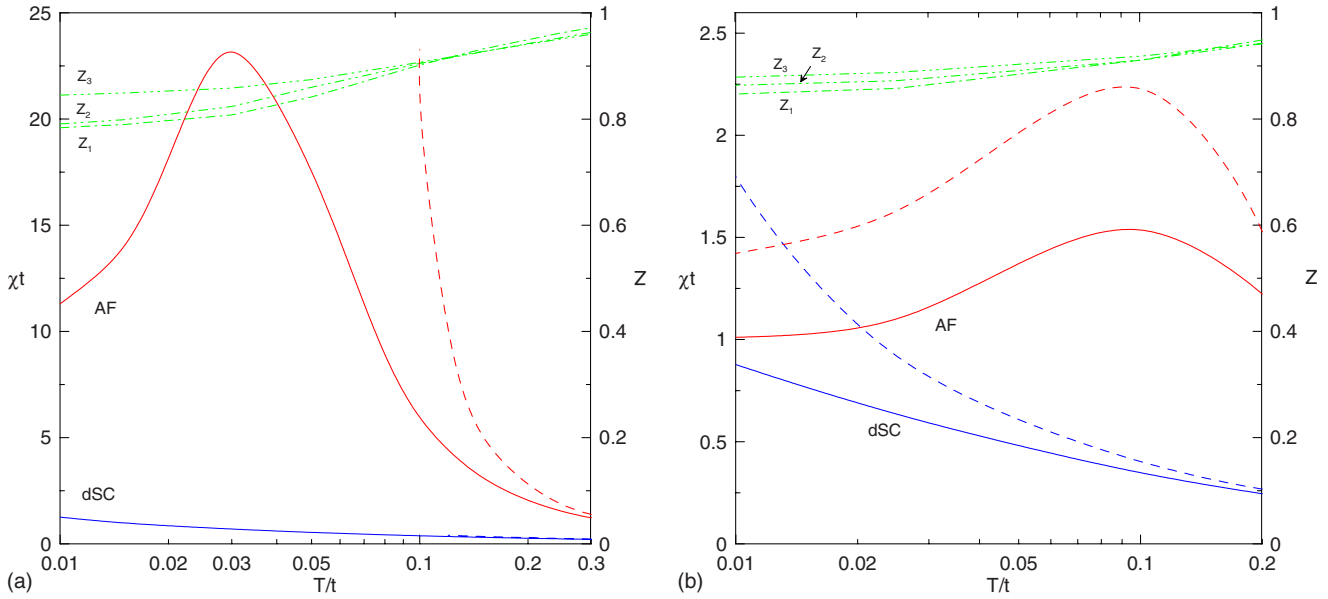

FIG. 8. (Color online) The temperature dependence of the antiferromagnetic and d-wave superconducting susceptibilities in one- (dashed lines) and two-loop (solid lines) functional renormalization group approaches to the 2D t-t' Hubbard model with $U=2t$, $t'/t=0.1$, (a) $\mu=0.1t$, and (b)$\mu=-0.1t$. The temperature dependence of the Z factors (right axis) is shown by dot-dashed lines; the number of dots corresponds to patch number.

however, required. At the same time, the quadratic temperature dependence at low temperatures supports the Fermi-liquid picture in this temperature range above the paramagnetic ground state. The Fermi surface shift contributions are small and negative for $\mu<0$. For $\mu>0$ the Fermi surface shifts have opposite signs at the point closest to the $(\pi,0)$ point and to the diagonal, leading therefore to small deformation of the Fermi surface, which makes it flatter.

IV. DISCUSSION AND CONCLUSIONS

We have considered the effect of the two-loop corrections on the fRG flow. In the 1D case we find that the nonuniversal corrections contribute to the flow at large momenta scales, while at small momentum scales we have recovered the results obtained from the field-theoretical RG approach. For the 2D case with flat Fermi surface we also find good agreement with the previous results of the field-theoretical RG. The fRG approach was applied further to the case of curved Fermi surface without nesting, where we obtained the flow of the vertices and susceptibilities at the two-loop level.

In two dimensions the two-loop corrections do not change the leading instability but may lead to a slight shift of the phase boundaries in comparison with the previous one-loop analysis. The difference of the two-loop results and the one-loop results with projected vertices in two dimensions is smaller than to the one-loop results with partly corrected projection errors and decreases going away from the van Hove band filling. Therefore, the commonly used one-loop fRG approach with projected vertices serves as a good starting point for calculating higher-loop corrections.

We have also considered the flow of the qp spectral weight, the qp damping, and the Fermi surface shift. In agreement with earlier studies, for curved Fermi surface and not too low temperatures in two dimensions we obtain the qp weight $Z\simeq 0.9$ so that the quasiparticles remain well defined during the fRG flow. The qp damping and estimated Fermi surface shifts are also numerically small. At the temperature close to the antiferromagnetic instability the spectral weight is suppressed and the pseudogap is formed, the description of this regime in the two-loop approach is, however, left beyond

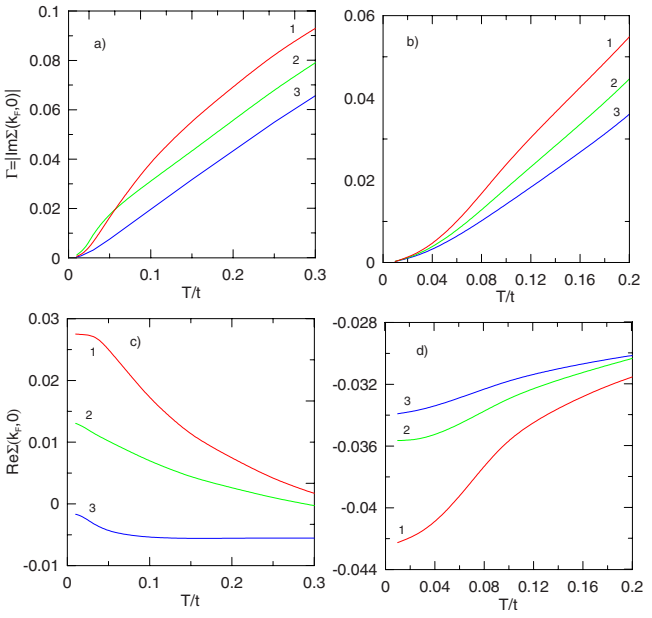

FIG. 9. (Color online) The temperature dependence of the (a) and (b) qp damping $\Gamma_{\mathbf{k}_F}=-\mathrm{Im}\,\Sigma(\mathbf{k}_F,0)$ and the (c) and (d) Fermi surface shift $\mathrm{Re}\,\Sigma(\mathbf{k}_F,0)/t$ at different Fermi surface patches (1, 2, and 3) obtained in the 24-patch two-loop fRG approach at $U=2t$ and $t'/t=0.1$; (a) and (c) $\mu=0.1t$ and (b) and (d)$\mu=-0.1t$. Patch 1 is the closest to the $(\pi,0)$ point.

the scope of the present paper because of the necessity of considering the frequency dependence of the self-energy (see e.g., Refs. 25 and 26).

Possible future applications of the method would be its implementation within the temperature-cutoff fRG scheme,[20] where the two-loop corrections are expected to be smaller than for momentum cutoff due to better treatment of degrees of freedom with different excitation energy. The calculation of the two-loop corrections for the temperature cutoff is, however, a more difficult task since it requires more intense numerical calculations caused by the smoothness of the cutoff. Another possible extension of the method would include consideration of the frequency dependence of the self-energy and/or vertices, which also has to be performed.

ACKNOWLEDGMENTS

We are grateful to W. Metzner for stimulating discussions and a careful reading of the manuscript. This work was supported in part by Russian Basic Research Foundation via support of Scientific Schools Grant No. (1941.2008.2) and Grant No. (07-02-01264a).

APPENDIX: DERIVATION OF THE TWO-LOOP FRG EQUATIONS

In this Appendix we consider the derivation of the two-loop RG equations. We use the notations of Refs. 18 and 19, which considered the 1PI RG equations for the terms of the expansion of the 1PI generating functional in fermionic field,

$$\Gamma_\Lambda(\phi) = \sum_{m\geq 0} \gamma_\Lambda^{(m)}(\phi)$$

where $\phi(X)$ are fermionic fields and

$$X = (x, \tau, \sigma, \pm) \tag{A1}$$

is the short notation for the space, time, spin, and charge variables (the $\pm$ sign corresponds to the incoming and the outgoing particles, respectively). At the two-loop order the hierarchy of RG equations for the 1PI functions is truncated at the three-particle vertex and has the form[18,19]

$$\dot\gamma_\Lambda^{(2)}(\phi) = (\phi, Q\phi) + \frac{1}{2}\mathrm{Tr}[S_\Lambda \tilde\gamma_\Lambda^{(2)}],$$

$$\dot\gamma_\Lambda^{(4)}(\phi) = \frac{1}{2}\mathrm{Tr}[S_\Lambda \tilde\gamma_\Lambda^{(4)}] - \frac{1}{2}\mathrm{Tr}[S_\Lambda \tilde\gamma_\Lambda^{(2)} G_\Lambda \tilde\gamma_\Lambda^{(2)}],$$

$$\dot\gamma_\Lambda^{(6)}(\phi) = -\frac{1}{2}\mathrm{Tr}[S_\Lambda \tilde\gamma_\Lambda^{(4)} G_\Lambda \tilde\gamma_\Lambda^{(2)} + S_\Lambda \tilde\gamma_\Lambda^{(2)} G_\Lambda \tilde\gamma_\Lambda^{(4)}] + \frac{1}{2}\mathrm{Tr}[S_\Lambda \tilde\gamma_\Lambda^{(2)} G_\Lambda \tilde\gamma_\Lambda^{(2)} G_\Lambda \tilde\gamma_\Lambda^{(2)}] + O(\gamma_\Lambda^{(8)}), \tag{A2}$$

where

$$\tilde\gamma_\Lambda^{(m)}(X, Y, \phi) = \frac{\delta}{\delta\phi(X)}\frac{\delta}{\delta\phi(Y)}\gamma_\Lambda^{(m+2)}(\phi). \tag{A3}$$

The trace is taken with respect to X-variables and dots denote derivatives with respect to Λ.

For practical calculations the vertices $\gamma_\Lambda^{(m)}(\phi)$ are expressed explicitly through the ϕ fields as

$$\gamma_\Lambda^{(m)}(\phi) = \frac{1}{m!}\sum_m \int dX^m \gamma_m(\Lambda|X)\phi(X_1)\ldots\phi(X_m) \tag{A4a}$$

and

$$\tilde\gamma_\Lambda^{(m)}(X, Y, \phi) = \frac{1}{m!}\int d^m X' \gamma_{m+2}(\Lambda|X, Y, X')\phi(X_1')\ldots\phi(X_m'). \tag{A4b}$$

In these notations the RG Eq. (12) reads as

$$\dot\gamma_2(\Lambda|X) = \frac{1}{2}\int d^2 Y \gamma_4(\Lambda|X, Y) S_\Lambda(Y), \tag{A5a}$$

$$\dot\gamma_4(\Lambda|X) = \frac{1}{2}\int d^2 Y \gamma_6(\Lambda|X, Y) S_\Lambda(Y) - \frac{1}{2}\int d^4 Y B_\Lambda(X, Y) L_\Lambda(Y), \tag{A5b}$$

$$\dot\gamma_6(\Lambda|X) = \frac{1}{2}\int d^6 Y D_\Lambda(X, Y) M_\Lambda(Y) - \frac{1}{2}\int d^4 Y E_\Lambda(X, Y) L_\Lambda(Y), \tag{A5c}$$

where

$$L_\Lambda(Y) = S_\Lambda(Y_1, Y_2) G_\Lambda(Y_3, Y_4) + G_\Lambda(Y_1, Y_2) S_\Lambda(Y_3, Y_4), \tag{A6}$$

$$B_\Lambda(X, Y) = \gamma_4(\Lambda|X_1 X_2; Y_2, Y_3)\gamma_4(\Lambda|X_3 X_4; Y_4, Y_1) - \gamma_4(\Lambda|X_1 X_3; Y_2, Y_3)\gamma_4(\Lambda|X_2 X_4; Y_4, Y_1) + \gamma_4(\Lambda|X_1 X_4; Y_2, Y_3)\gamma_4(\Lambda|X_2 X_3; Y_4, Y_1), \tag{A7}$$

and

$$M_\Lambda(Y) = S_\Lambda(Y_1, Y_2) G_\Lambda(Y_3, Y_4) G_\Lambda(Y_5, Y_6) + G_\Lambda(Y_1, Y_2) S_\Lambda(Y_3, Y_4) G_\Lambda(Y_5, Y_6) + G_\Lambda(Y_1, Y_2) G_\Lambda(Y_3, Y_4) S_\Lambda(Y_5, Y_6), \tag{A8}$$

$$D_\Lambda(X, Y) = \gamma_4(\Lambda|X_1, X_2; Y_2 Y_3)\gamma_4(\Lambda|X_3 X_4; Y_4 Y_5) \times \gamma_4(\Lambda|X_5 X_6; Y_6 Y_!) + 14 \text{ permutations}, \tag{A9}$$

$$E_\Lambda(X, Y) = \gamma_4(\Lambda|X_1 X_2; Y_2 Y_3)\gamma_6(\Lambda|X_3 X_4 X_5 X_6; Y_4 Y_1) + 14 \text{ permutations}, \tag{A10}$$

As discussed in main text, in the present paper we consider the expansion in the number of loops rather than in effective vertices. Iterating Eq. (A5c) for $\gamma^{(6)}$, one can easily see that the first term in this equation corresponds to the three-loop contribution to $\gamma^{(4)}$. Therefore, in the following we neglect this term. Due to this neglect, Eq. (A5c) can be

integrated analytically. Substituting the result into Eq. (A5b) we obtain

$$\dot{\gamma}_2(\Lambda|X) = \frac{1}{2}\int d^2Y \gamma_4(\Lambda|X,Y)S_\Lambda(Y),$$

$$\dot{\gamma}_4(\Lambda|X) = \frac{1}{4}\int_\Lambda^{\Lambda_0} d\Lambda' \int d^2Y \int d^6Y' S_\Lambda(Y) M_\Lambda(Y') \times D_\Lambda[(X,Y),Y'] - \frac{1}{2}\int d^4Y L_\Lambda(Y) B_\Lambda(X,Y). \tag{A11}$$

This substitution considerably simplifies the numerical solution of the equations since one has to consider the vertices γ_2 and γ_4 only.

Introducing the self-energy and two-particle irreducible vertex by

$$\Sigma(\xi_1,\xi_2) = \gamma_2[(\xi_1,\uparrow,+),(\xi_2,\uparrow,-)],$$

$$V(\xi_1\xi_2;\xi_3\xi_4) = \gamma_4[(\xi_1,\uparrow,+),(\xi_2,\downarrow,+),(\xi_3,\uparrow,-),(\xi_4,\downarrow,-)], \tag{A12}$$

where $\xi_i=(\mathbf{x}_i,\tau_i)$ and the Fourier transformed quantities

$$\Sigma(k) = \int d^2\xi \Sigma(\xi_1,\xi_2) e^{i(\xi_1-\xi_2)k},$$

$$V(k_1k_2;k_3k_4) = \int d^4\xi V(\xi_1\xi_2;\xi_3\xi_4) e^{i\xi_1k_1+i\xi_2k_2-i\xi_3k_3-i\xi_4k_4}, \tag{A13}$$

where $k_i=(\mathbf{k}_i, i\omega_n^{(i)})$ and exploiting charge-, spin-, and translational invariance in the same way as in Refs. 18 and 19 we obtain Eqs. (A5a)–(A5c) of the paper.

Similar derivation can be performed for susceptibilities. Following Ref. 19 we introduce vertices $\gamma_\Lambda^{(m,n)}$ where m refers to the number of boson lines and n to the number of fermion lines, which enter or go out of the vertex. The equations for the vertices $\gamma_\Lambda^{(m,n)}$ read

$$\dot{\gamma}_\Lambda^{(2,0)}(\phi) = \frac{1}{2}\mathrm{Tr}[S_\Lambda \tilde{\gamma}_\Lambda^{(1,0)} G_\Lambda \tilde{\gamma}_\Lambda^{(1,0)} G_\Lambda], \tag{A14}$$

$$\dot{\gamma}_\Lambda^{(1,2)}(\phi) = -\frac{1}{2}\mathrm{Tr}[S_\Lambda \tilde{\gamma}_\Lambda^{(1,2)}] + \frac{1}{2}\mathrm{Tr}[S_\Lambda \tilde{\gamma}_\Lambda^{(1,0)} G_\Lambda \tilde{\gamma}_\Lambda^{(0,2)}], \tag{A15}$$

$$\dot{\gamma}_\Lambda^{(1,4)}(\phi) = -\frac{1}{2}\mathrm{Tr}[S_\Lambda \tilde{\gamma}_\Lambda^{(1,4)}] + \frac{1}{2}\mathrm{Tr}[S_\Lambda \tilde{\gamma}_\Lambda^{(1,0)} G_\Lambda \tilde{\gamma}_\Lambda^{(0,4)}] + \frac{1}{2}\mathrm{Tr}[S_\Lambda \tilde{\gamma}_\Lambda^{(1,2)} G_\Lambda \tilde{\gamma}_\Lambda^{(0,2)}] + \frac{1}{2}\mathrm{Tr}[S_\Lambda \tilde{\gamma}_\Lambda^{(1,0)} G_\Lambda \tilde{\gamma}_\Lambda^{(0,2)} G_\Lambda \tilde{\gamma}_\Lambda^{(0,2)}]. \tag{A16}$$

Expanding again $\gamma^{(m,n)}(\phi)$ in ϕ, neglecting the first three terms in the equation for $\dot{\gamma}_\Lambda^{(1,4)}(\phi)$ as corresponding to the higher-loop order, and substituting the result for $\dot{\gamma}_\Lambda^{(1,4)}(\phi)$ in the equation for $\dot{\gamma}_\Lambda^{(1,2)}(\phi)$, we obtain

$$\dot{\gamma}^{(1,0)}(\Lambda|X,X') = \int d^4Y L_\Lambda(Y) \gamma^{(1,2)}(\Lambda|X,Y_2,Y_3) \gamma^{(1,2)} \times (\Lambda|X',Y_4,Y_1), \tag{A17}$$

$$\dot{\gamma}^{(1,2)}(\Lambda|X,X') = \frac{1}{4}\int_\Lambda^{\Lambda_0} d\Lambda' \int d^2Y \int d^6Y' S_\Lambda(Y) M_\Lambda(Y') \times \tilde{D}_\Lambda[X,(X',Y),Y'] - \frac{1}{2}\int d^4Y L_\Lambda(Y) \tilde{B}_\Lambda(X,X',Y), \tag{A18}$$

where

$$\tilde{B}_\Lambda(X,X',Y) = \gamma_{(1,2)}(\Lambda|X;Y_2,Y_3)\gamma_4(\Lambda|X_1'X_2';Y_4,Y_1), \tag{A19}$$

$$\tilde{D}_\Lambda(X,X',Y) = \gamma_{(1,2)}(\Lambda|X;Y_2Y_3)\gamma_4(\Lambda|X_1'X_2';Y_4Y_5) \times \gamma_4(\Lambda|X_3'X_4';Y_6Y_!) + \text{permutations } (X'), \tag{A20}$$

[1] W. Metzner and D. Vollhardt Phys, Phys. Rev. Lett. **62**, 324 (1989); A. Georges, G. Kotliar, W. Krauth, and M. J. Rozenberg, Rev. Mod. Phys. **68**, 13 (1996).
[2] H. Q. Lin and J. E. Hirsch, Phys. Rev. B **35**, 3359 (1987).
[3] J. Solyom, Adv. Phys. **28**, 201 (1979).
[4] J. Kanamori, Prog. Theor. Phys. **30**, 275 (1963).
[5] A. Liebsch, Phys. Rev. B **23**, 5203 (1981).
[6] M. I. Katsnelson and A. I. Lichtenstein, J. Phys.: Condens. Matter **11**, 1037 (1999); Eur. Phys. J. B **30**, 9 (2002).
[7] Y. M. Vilk and A. M.-S. Tremblay, J. Phys. I **7**, 1309 (1997).
[8] N. E. Bickers and D. J. Scalapino, Ann. Phys. **193**, 206 (1989).
[9] N. E. Bickers and S. R. White, Phys. Rev. B **43**, 8044 (1991).
[10] V. Janis, J. Phys.: Condens. Matter **10**, 2915 (1998).
[11] V. Janis, Phys. Rev. B **60**, 11345 (1999).
[12] This general form of the parquet approach should be, however, distinguished from the "fast parquet approach" of Ref. 13 where only vertex corrections in the leading logarithmic approximation are taken into account and the self-energy corrections are not considered.
[13] I. E. Dzyaloshinskii and V. M. Yakovenko, Zh. Eksp. Teor. Fiz. **94**, 344 (1988) [Sov. Phys. JETP **67**, 844 (1988)]; Int. J. Mod. Phys. B **2**, 667 (1988); A. T. Zheleznyak, V. M. Yakovenko, and I. E. Dzyaloshinskii, Phys. Rev. B **55**, 3200 (1997).
[14] J. Polchinski, Nucl. Phys. B **231**, 269 (1984).

[15] D. Zanchi and H. J. Schulz, Phys. Rev. B **54**, 9509 (1996); **61**, 13609 (2000).
[16] M. Salmhofer, *Renormalization* (Springer, Berlin, 1999).
[17] C. J. Halboth and W. Metzner, Phys. Rev. B **61**, 7364 (2000).
[18] C. Honerkamp, M. Salmhofer, N. Furukawa, and T. M. Rice, Phys. Rev. B **63**, 035109 (2001).
[19] M. Salmhofer and C. Honerkamp, Prog. Theor. Phys. **105**, 1 (2001).
[20] C. Honerkamp and M. Salmhofer, Phys. Rev. Lett. **87**, 187004 (2001); Phys. Rev. B **64**, 184516 (2001).
[21] C. Honerkamp, D. Rohe, S. Andergassen, and T. Enss, Phys. Rev. B **70**, 235115 (2004).
[22] A. A. Katanin and A. P. Kampf, Phys. Rev. B **68**, 195101 (2003).
[23] A. P. Kampf and A. A. Katanin, Phys. Rev. B **67**, 125104 (2003).
[24] C. Honerkamp and M. Salmhofer, Phys. Rev. B **67**, 174504 (2003).
[25] A. A. Katanin and A. P. Kampf, Phys. Rev. Lett. **93**, 106406 (2004).
[26] D. Rohe and W. Metzner, Phys. Rev. B **71**, 115116 (2005).
[27] H. Freire, E. Correa, and A. Ferraz, Phys. Rev. B **71**, 165113 (2005); **78**, 125114 (2008); **78**, 195108 (2008).
[28] P. Kopietz, Nucl. Phys. B **595**, 493 (2001).
[29] V. Yu. Irkhin, A. A. Katanin, and M. I. Katsnelson, Phys. Rev. B **64**, 165107 (2001).
[30] A. A. Katanin, Phys. Rev. B **70**, 115109 (2004).
[31] C. Honerkamp, Eur. Phys. J. B **21**, 81 (2001).
[32] T. Nomura and K. Yamada, J. Phys. Soc. Jpn. **72**, 2053 (2003).
[33] A. Neumayr and W. Metzner, Phys. Rev. B **67**, 035112 (2003).
[34] M. Salmhofer, Ann. Phys. **16**, 171 (2007).
[35] H. Freire (private communication).
[36] Above the antiferromagnetic instability (for smaller $|\mu|$), the behavior of the Z factors is similar to that observed for the nested Fermi surface case: at sufficiently low temperatures close to the temperature of vertex divergence they are suppressed down to small values and the approximation of Eq. (14) breaks down.